Journal of Applied Mechanics and Technical Physics, Vol. 49, No. 5, pp. 712–722, 2008

COMPACTION OF A MIXTURE OF COPPER AND MOLYBDENUM NANOPOWDERS MODELED BY THE MOLECULAR DYNAMICS METHOD

S. P. Kiselev

UDC 539.3+539.412

A problem of compacting a mixture of copper and molybdenum nanopowders under the action of external loading generated by a spherical piston is solved by the molecular dynamics method. Interatomic interaction is calculated with the use of a multiparticle potential obtained by the embedded atom method. It is shown that compaction leads to significant deformations in copper, resulting in the loss of the crystalline structure; copper nanoparticles melt and fill the entire porous space. Molybdenum particles are deformed to a much smaller extent; they are not destroyed and preserve their crystalline structure. Under high loading, there appear voids in copper at the stage of compact extension; these voids rapidly grow in size and coagulate into one large void located in the nanocell center.

Key words: *nanoparticles, voids, copper, molybdenum, molecular dynamics, pressure, temperature.*

Introduction. One promising method of obtaining new materials is compaction of micro- and nanopowders in shock waves [1–3]. The energy applied to a system at the macroscopic level is transferred to the nanoscopic level, where it is transformed to the energy of bonding of atoms forming the compact. The difficulties arising in mathematical modeling of nanopowder compaction are caused by the wide range of scales of the processes playing a significant role in compaction. An approximate technique, which allows these difficulties to be overcome, was proposed in [4, 5] by an example of copper nanopowder compaction. First, the problem of compacting a nanocell under pulsed loading is solved by the molecular dynamics method. The solution obtained is averaged and yields the mean parameters, which allow the structure of the compact being formed to be determined. In the present work, this approach is extended to a mixture of copper (Cu) and molybdenum (Mo) powders. These materials were chosen because composites obtained by the method of explosive compaction from a mixture of Cu and Mo powders display high erosion resistance and are used for production of electrodes [6, 7]. In addition, a detailed metallographic research of the Cu–Mo composite structure is reported in [7], and the calculated results can be compared with the experimental data [7].

Formulation of the Problem. Let us consider a problem of compacting a spherical nanocell under pulsed loading applied to the outer surface of the piston (Fig. 1). Pulsed loading is transferred to the nanocell owing to interaction of the inner surface of the piston with atoms in the nanocell. The nanocell consists of four spherical Cu nanoparticles and four Mo nanoparticles of radius R_p with dense cubic packing. The centers of the Cu and Mo particles are located in the vertices of a cube with a rib length l. There are voids in the nanocell center and on the side faces of the cube. The volume of the void located on the side face of the cube is half the volume of the void in the cube center.

Khristianovich Institute of Theoretical and Applied Mechanics, Siberian Division, Russian Academy of Sciences, Novosibirsk 630090; kiselev@itam.nsc.ru. Translated from Prikladnaya Mekhanika i Tekhnicheskaya Fizika, Vol. 49, No. 5, pp. 11–23, September–October, 2008. Original article submitted July 30, 2007.

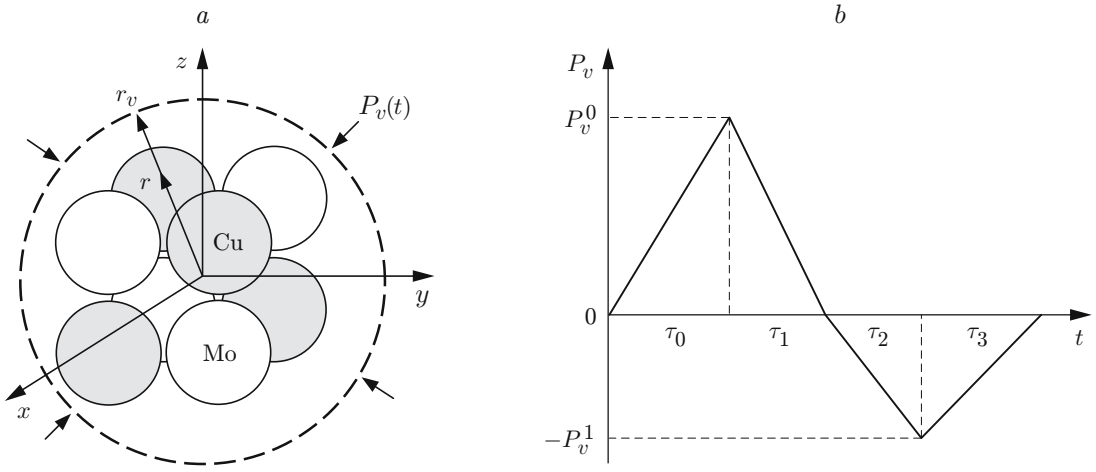

Fig. 1. Loading of a Cu–Mo nanocell by a pressure pulse $P_v(t)$; the arrows show the applied external pressure $P_v(t)$; the dashed line indicates the spherical piston: (a) nanocell; (b) pressure pulse.

We use the molecular dynamics method to calculate the nanocell deformation under the action of the spherical piston [8]. The motion of copper and molybdenum atoms is described by the Hamilton equations [8] with the Hamiltonian

$$H = K + \sum_{a=1}^{N} V_{\text{ext}}(x_{ai}) + U(x_{ai}), \qquad K = \sum_{a=1}^{N}\sum_{i=1}^{3} \frac{p_{ai}^2}{2m_a}, \tag{1}$$

where p_{ai} and x_{ai} are the pulses and coordinates of atoms (a is the atom number, and i is the coordinate number), m_a and N are the mass and the total number of atoms, respectively, K is the kinetic energy, and U and V_{ext} are the potentials of interatomic interaction and external forcing. The potential of interatomic interaction U was chosen to be the multiparticle Cleri–Rosato potential [9, 10] calculated by the embedded atom method:

$$U = \sum_{a=1}^{N} F(\rho_a) + \sum_{a=1}^{N}\sum_{b\neq a}^{N} \varphi(r_{ab}), \qquad \rho_a = \sum_{b\neq a}^{N} f(r_{ab}), \qquad F(\rho_a) = -\sqrt{\rho_a},$$
$$f(r_{ab}) = \xi^2 \exp\left(-2q(r_{ab}/r_0 - 1)\right), \qquad \varphi(r_{ab}) = A\exp\left(-p(r_{ab}/r_0 - 1)\right). \tag{2}$$

Here ρ_a is the electron density at the point where the atom a is located and r_{ab} is the distance between the atoms a and b. The first term in the right side of the first equation in (2) describes attraction of atoms due to their interaction with the electron gas, and the second term describes repulsion of positively charged atoms due to the Coulomb interaction. The second equation in (2) defines the electron density in the atom a generated by the remaining atoms. Interaction of Cu and Mo atoms was also calculated by Eqs. (2) with the following approximation for the potentials [10, 11]:

$$f_{\text{CuMo}}(r_{ab}) = \sqrt{f_{\text{Cu}}(r_{ab}) f_{\text{Mo}}(r_{ab})}, \qquad \varphi_{\text{CuMo}}(r_{ab}) = \sqrt{\varphi_{\text{Cu}}(r_{ab})\varphi_{\text{Mo}}(r_{ab})}.$$

Potential (2) was cut so that the functions f and φ, as well as their first derivatives, were continuous at the cut-off point r_c. The calculations included interaction of atoms located within three coordination spheres; hence, the cut-off radius was $r_c = 4.82$ Å.

Expanding the function $F(\rho_a)$ into a series in the neighborhood of the equilibrium state as

$$F(\rho_a) \approx F(\rho_a^0) + \frac{1}{2\sqrt{\rho_a^0}} \sum_b f(r_{ab}) + \sum_{b,c} c_{bc} f(r_{ab}) f(r_{ac}) + \ldots$$

and retaining terms proportional to the first power of f, we write the first equation in (2) in the form

$$U \approx \frac{1}{2}\sum_{a=1}^{N}\sum_{b\neq a}^{N} V(r_{ab}) + \ldots, \qquad V(r_{ab}) \approx 2\varphi(r_{ab}) - \frac{f(r_{ab})}{\sqrt{\rho_a^0}},$$

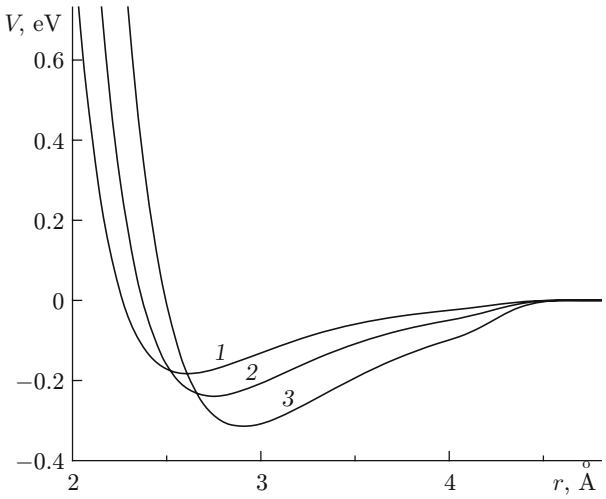

Fig. 2. Effective pair potentials Cu–Cu (1), Cu–Mo (2), and Mo–Mo (3).

where the function $V(r_{ab})$ has the meaning of an effective pair potential and ρ_a^0 is the electron density in the equilibrium state [10, 11]. In the present work, we used the constants A, p, q, ξ, and r_0 for Cu and Mo atoms [10], which allowed us to calculate the effective pair potentials (Fig. 2). It is seen that the minimum of the effective interaction potential $V(r_{\mathrm{MoMo}})$ (curve 3) for molybdenum atoms is lower than that for copper atoms $V(r_{\mathrm{CuCu}})$ (curve 1), and the minimum of the potential of interaction between copper and molybdenum $V(r_{\mathrm{CuMo}})$ (curve 2) lies between these curves. This means that the bond between molybdenum atoms is stronger than the bond between copper atoms, whereas the bond between copper and molybdenum atoms is of intermediate strength.

Interaction of piston atoms x_v with nanocell atoms x_a was modeled by an external potential, which was chosen in the form of the Lennard-Jones potential

$$V_{LJ} = D(x^{-12} - 2x^{-6}), \qquad x = R/d,$$

where $R = \sqrt{(x_a^1 - x_v^1)^2 + (x_a^2 - x_v^2)^2 + (x_a^3 - x_v^3)^2}$ is the distance between the atoms, D is the depth of the potential well, and d is the distance at which the minimum energy is reached.

We assume that the piston consists of Cu atoms occupying a fraction of a unit volume ω_1 and Mo atoms occupying a fraction of a unit volume ω_2. Cu atoms are located in the nodes of a face-centered cubic (FCC) lattice with a lattice constant a_1 and mean density $4/a_1^3$, and Mo atoms are located in the nodes of a body-centered cubic (BCC) lattice with a lattice constant a_2 and mean density $2/a_2^3$. To find the potential of interaction of the x_ath atom of the nanocell with the piston V_{ext}, we have to sum up V_{LJ} over all x_v atoms of the piston. Replacing summation by integration, as it was done in [12], we find

$$V_{\mathrm{ext},\alpha}(x_a) = \sum_{\beta=1}^{2} A_{\alpha,\beta}\Big(\Big(\frac{d_{\alpha,\beta}}{s}\Big)^9 - 15\Big(\frac{d_{\alpha,\beta}}{s}\Big)^3\Big),$$

$$s = |r - r_v|, \qquad r = \sqrt{(x_a^1)^2 + (x_a^2)^2 + (x_a^3)^2}, \tag{3}$$

$$A_{1,1} = \frac{\sqrt{2}\pi}{45} D_{1,1}\omega_1, \quad A_{1,2} = \frac{\sqrt{3}\pi}{60} D_{1,2}\omega_2, \quad A_{2,1} = \frac{\sqrt{2}\pi}{45} D_{1,2}\omega_1, \quad A_{2,2} = \frac{\sqrt{3}\pi}{60} D_{2,2}\omega_2,$$

where $d_{\alpha,\beta}$ and $D_{\alpha,\beta}$ are the coordinate of the minimum interaction energy and the depth of the potential well, respectively, for Cu–Cu, Cu–Mo, and Mo–Mo pairs determined from the corresponding curves of the effective pair potentials (see Fig. 2). In the present work, $\alpha = 1$ and $\alpha = 2$ refer to copper and molybdenum, respectively. As the main contribution to potential (3) is made by atoms located near the piston surface in a thin layer of the order of r_c much smaller than the piston radius ($r_c \ll r_v$), the piston curvature was neglected in deriving Eq. (3). The piston radius r_v and velocity v_v are found from the equations of motion

$$\frac{dp_v}{dt} = \sum_{a=1}^{N} \tilde{F}_a - 4\pi r_v^2 P_v(t), \qquad \frac{dr_v}{dt} = v_v, \qquad p_v = M_v v_v,$$

$$\tilde{F}_a = -\frac{\partial V_{\text{ext}}(s_a)}{\partial r_a}, \qquad s_a = |r_a - r_v|,$$

where $P_v(t)$ is the pressure and $M_v = 4\pi(r_v^0)^2 h_v \rho_v$ and $\rho_v = 4\omega_1 m_1/a_1^3 + 2\omega_2 m_2/a_2^3$ are the mass and density of the piston, respectively.

A system of ordinary differential equations of motion of atoms and the piston was solved numerically on the basis of the Verlet scheme [8]. As a result, we found the atom pulses and coordinates and, based on these values, determined the mean pressure P_α, temperature T_α, and density ρ_α in the species ($\alpha = 1, 2$) and in the nanocell:

$$P_\alpha = \frac{1}{3V} \sum_{a=1}^{N_\alpha} \sum_{i=1}^{3} (m_\alpha v'_{ai} v'_{ai} + F_a^i x_a^i), \quad T_\alpha = \frac{2}{3N_\alpha k_{\text{B}}} \sum_{a=1}^{N_\alpha} \sum_{i=1}^{3} \frac{m_\alpha v'_{ai} v'_{ai}}{2}, \quad \rho_\alpha = \frac{M_\alpha}{V_\alpha},$$

$$P = P_1 + P_2, \quad T = c_1 T_1 + c_2 T_2, \quad \rho_s = \omega_1 \rho_1 + \omega_2 \rho_2, \quad \rho = M/(V + V_d), \quad M_\alpha = N_\alpha m_\alpha,$$

$$N = N_1 + N_2, \quad V = V_1 + V_2, \quad M = M_1 + M_2, \quad c_\alpha = N_\alpha/N, \quad \omega_\alpha = V_\alpha/V,$$

$$v'_{ai} = v_{ai} - \langle v_{ai} \rangle, \quad \langle v_{ai} \rangle = \frac{1}{N} \sum_{a=1}^{N} v_{ai}, \quad F_a^i = \sum_{b \neq a}^{N} F_{ab}^i, \quad x_{ab}^i = x_a^i - x_b^i, \quad F_{ab}^i = -\frac{\partial U}{\partial x_{ab}^i}.$$

Here k_{B} is the Boltzmann constant, V is the volume occupied by atoms, V_d is the volume occupied by voids in the nanocell, ρ is the mean density of the porous material, ρ_s is the mean density of the solid material, and V_α, N_α, and M_α are the volume, number of atoms, and mass of the α-species, respectively. The accuracy of satisfaction of the energy conservation law was monitored during the numerical calculations. The work performed by the applied external pressure $\Delta A_v = -\int\limits_{V_0}^{V} P_v \, dV = 4\pi \int\limits_{r_v}^{r_v^0} P_v r_v^2 \, dr_v$ equals the increment of the total energy of the system of atoms and the piston $\Delta E = E(t) - E(0)$, where $E = M_v v_v^2/2 + H$ [the quantity H was defined in Eq. (1)]. The accuracy of satisfaction of the energy conservation law is characterized by the quantity $\delta E = \Delta E - \Delta A_v$ whose dimensionless value in numerical calculations performed with a time step of 2.5 fsec is within $\delta E/E \leqslant 0.5\%$.

Before the nanocell was loaded by a pressure pulse, an equilibrium structure was formed, which was considered as the initial structure prior to nanocell loading. Copper atoms were located in the nodes of an ideal FCC lattice with a lattice constant $a_1 = 3.62$ Å, whereas molybdenum atoms were located in the nodes of an ideal BCC lattice with a lattice constant $a_2 = 3.147$ Å. The total number of atoms in four copper nanoparticles was $N_1 = 3900$, and the total number of atoms in four molybdenum particles was $N_2 = 2900$. The Cu and Mo particles had identical radii: $R_p = 1.4$ nm, and the distance between the centers of the neighboring nanoparticles was $l = 4$ nm. The minimum distance between the atoms from different nanoparticles was greater than 3.62 Å, and interaction of nanoparticles at the stage of formation of the initial configuration could be eliminated. After that, a preliminary calculation was performed with the temperature in the nanocell atoms increased to $T_0 = 300$ K under the action of random forcing.

The nanocell was loaded by a spherical piston whose outer surface was subjected to pressure $P_v(t)$. At the initial time ($t = 0$), the spherical piston was at rest ($v_v = 0$) and had a radius $r_v^0 = 47.3$ Å. The piston mass M_v was 1.5 times the total mass of atoms M_s in the nanocell ($M_v/M_s = 1.49$).

Discussion of Numerical Results. Figures 3 and 4 show the calculated deformation of the nanocell loaded by a pressure pulse with the following parameters: $P_v^0 = 1$ GPa, $P_v^1 = 0.3$ GPa, $\tau_0 = 2 \cdot 10^3$ fsec, $\tau_1 = 8 \cdot 10^3$ fsec, $\tau_2 = 2 \cdot 10^3$ fsec, and $\tau_3 = 3 \cdot 10^3$ fsec. In this case, the mean strain rate was $\dot{\varepsilon} \approx (1 - r_v/r_v^0)/\Delta t \approx 6 \cdot 10^{10}$ sec^{-1}.

The process of nanocell compaction can be divided into three stages. At the first stage ($t \leqslant 2 \cdot 10^3$ fsec), the nanoparticles are compacted to the state of dense packing. Under the action of the piston, each nanoparticle starts to move toward the center, and then it is reflected and moves back to the piston; at this stage, the nanoparticles are not deformed (see Fig. 3a). At the second stage, the voids become filled, and a compact in the Cu–Mo system is formed. The process of void filling has an oscillatory character. As a result of nanocell compression, the pressure in

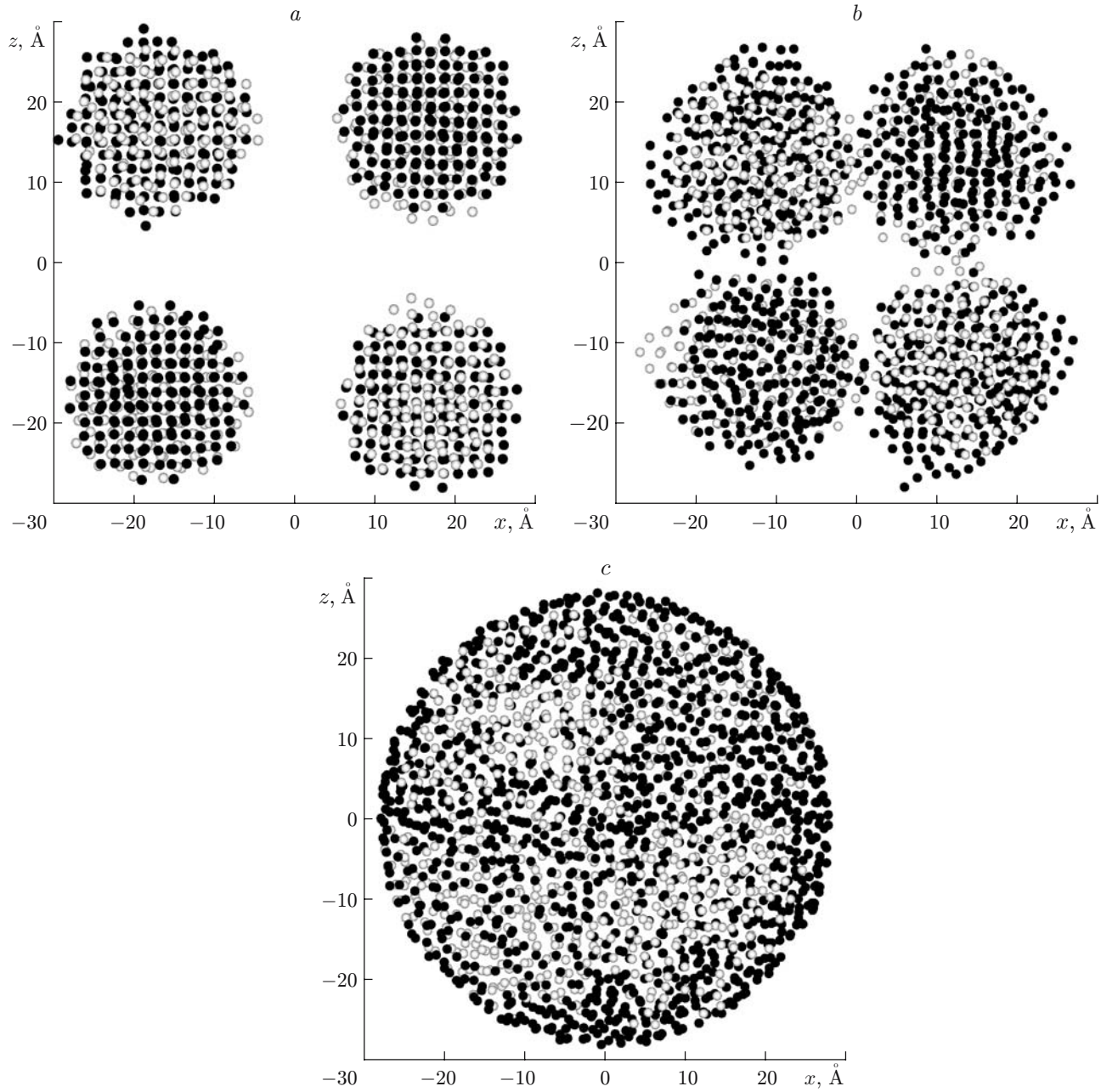

Fig. 3. Projection of nanocell atoms located in the layer -4 Å $< y < 4$ Å onto the plane (x, z) at different times (pressure pulse $P_v^0 = 1$ GPa and $P_v^1 = 0.3$ GPa): (a) $t = 1.2 \cdot 10^3$ fsec; (b) $t = 6 \cdot 10^3$ fsec; (c) $t = 1.2 \cdot 10^4$ fsec; the black and white circles are the Cu and Mo atoms, respectively.

the nanoparticles increases. As the pressure reaches $P \approx 1.5$ GPa, plastic deformation starts in the nanoparticles, which leads to changes in the particle shape (see Fig. 3b) and pressure relaxation in the nanocell. This process is repeated until all voids are filled; as a result, a number of pressure peaks appear (see Fig. 4b) at the times $t = 3 \cdot 10^3$, $4 \cdot 10^3$, and $5 \cdot 10^3$ fsec. The copper nanoparticles becomes destroyed, and copper atoms fill the voids; the molybdenum nanoparticles are strongly deformed, but they still stay compact (see Fig. 3c). At the third stage ($t \geqslant 8 \cdot 10^3$ fsec), the nanocell experiences weakly decaying oscillations with a period $\tau_v \approx 4 \cdot 10^3$ fsec (see Fig. 4a and 4b). The nanocell acquires a spherical shape and has no voids (see Figs. 3c and 4f). The amplitude of oscillations is determined by the stored kinetic energy of the nanoparticles after void filling, and the period of oscillations is

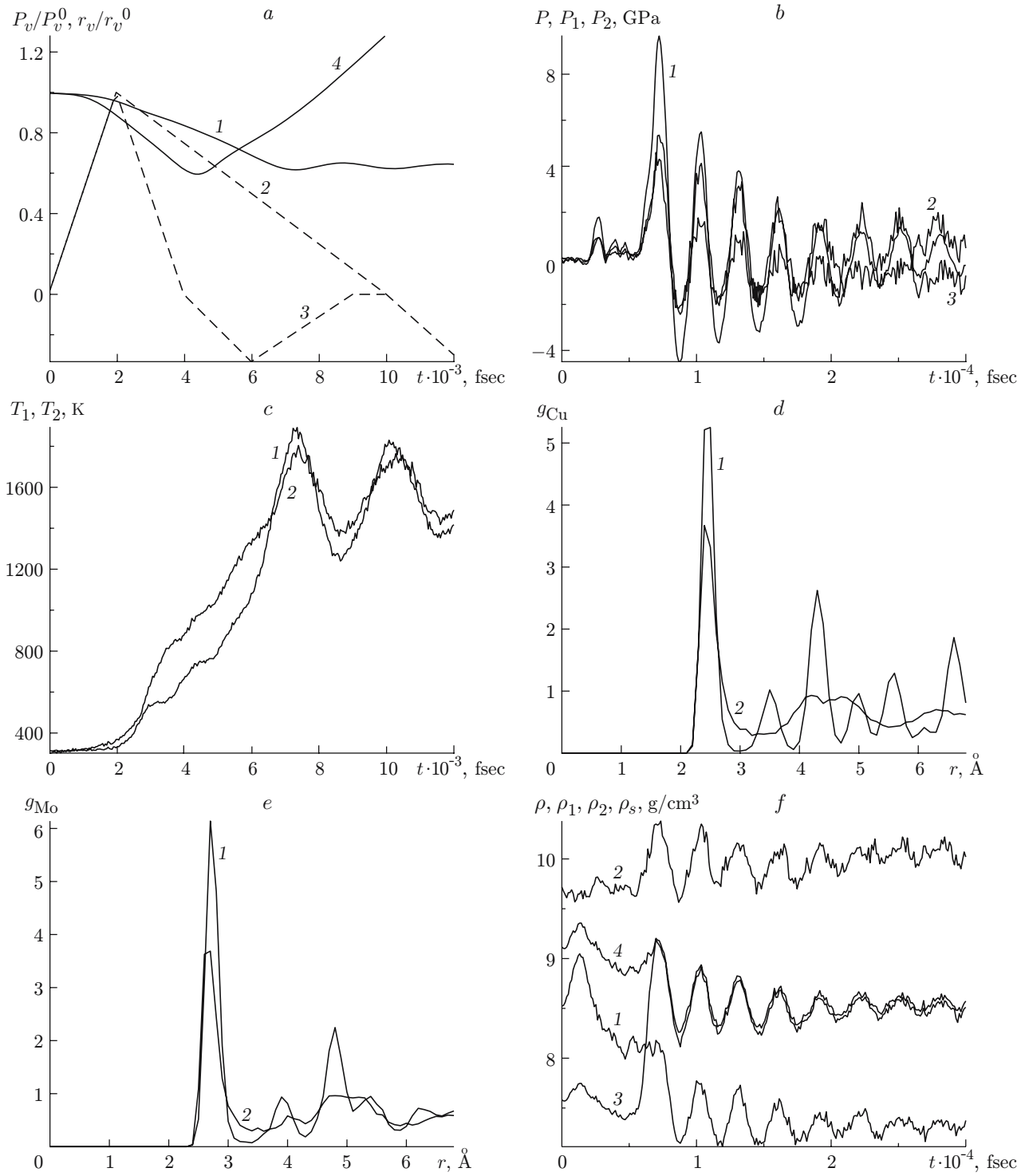

Fig. 4. Calculated mean parameters of the Cu–Mo nanocell: (a) $r_v(t)/r_v^0$ (solid curves) and $P_v(t)/P_v^0$ (dashed curves), curves 1 and 2 are the results calculated for $P_v^0 = 1$ GPa and $P_v^1 = 0.3$ GPa, and curves 3 and 4 are the results calculated for $P_v^0 = 3.6$ GPa and $P_v^1 = 1.2$ GPa; (b)–(f) calculations of the nanocell loaded by a pressure pulse $P_v^0 = 1$ GPa and $P_v^1 = 0.3$ GPa; (b) $P(t)$ (1), $P_1(t)$ (2), and $P_2(t)$ (3); (c) $T_1(t)$ (1) and $T_2(t)$ (2); (d) radial distribution function in copper for $t = 1.2 \cdot 10^3$ (1) and $1.2 \cdot 10^4$ fsec (2) and after nanocell cooling; (e) radial distribution function in molybdenum for $t = 1.2 \cdot 10^3$ (1) and $1.2 \cdot 10^4$ fsec (2); (f) $\rho_1(t)$ (1), $\rho_2(t)$ (2), $\rho(t)$ (3), and $\rho_s(t)$ (4).

determined by the inertial and elastic properties of the nanocell–piston mechanical system. The characteristic time of oscillations τ_v is approximately thrice greater than the characteristic time of propagation of compression and expansion waves in the nanocell: $\tau_c \approx 2R_s/c \approx 1.4 \cdot 10^3$ fsec ($R_s \approx 28$ Å is the nanocell radius and $c \approx 4 \cdot 10^3$ m/sec is the bulk velocity of sound in copper).

Let us consider the first two stages of compaction in more detail. It is seen in Fig. 4c that the increase in temperature in the nanocell occurs at the second stage and is caused by plastic strains in the nanoparticles. The temperature of the Mo nanoparticles is a monotonically increasing function of time, and the increase in temperature of the Cu nanoparticles has a stepwise character (see Fig. 4c). An analysis of the atomic configurations shows that the presence of plateaus on the dependence $T_1(t)$ at $t \leqslant 5 \cdot 10^3$ fsec in the Cu nanoparticles is caused by the formation of an amorphous structure in regions on the boundaries with the piston and nanoparticles. Plastic strains appear in these regions, which leads to pressure relaxation (see Fig. 4b). During the process of void filling, the temperature in the Cu nanoparticles (see Fig. 4c) is higher than the melting point of copper $T_m = 1356$ K; hence, the Cu nanoparticles at the third stage are in the melted state and lose their spherical shape; thus, copper atoms are disseminated over the entire nanocell volume. The Mo nanoparticles remain compact during the entire loading process. Figures 4d and 4e show the radial distribution functions $g_\alpha(r)$ in the copper and molybdenum species [$g_\alpha(r) = (dN_\alpha(r)/dr)/(4\pi r^2 N_\alpha n_\alpha)$, where r is the distance between the atoms and $dN_\alpha(r)$ is the number of atoms in the spherical layer $(r, r + dr)$] for two times: at the beginning of loading and after nanocell cooling. Copper is seen to completely lose its crystalline structure and to pass to the amorphous state during the deformation process. The radial distribution function for molybdenum after compaction and nanocell cooling has "smeared" maximums in the second and third coordination spheres; hence, in addition to regions with an amorphous structure in the Mo nanoparticles, there are also regions where the crystalline structure of the material is retained.

It should be noted that the behavior of density of the species in the Cu–Mo mixture during its compaction is rather unusual. It is seen from Fig. 4f that, for the case of nanocell compression, the dependence of the density of the Mo species on time $\rho_2(t)$ is similar to the dependence $P(t)$ (see Fig. 4b), whereas the dependence of density of the Cu species on time $\rho_1(t)$ at the first two stages of compression behaves in the opposite manner. With increasing pressure P, the density of copper decreases, and the dependence $\rho_1(t)$ displays two drops of density. The first drop is caused by the emergence of an amorphous structure (having a lower density) during plastic deformation. The second fall of the copper density is caused by copper heating and melting during void filling. At the third stage, we see gradually decaying density oscillations caused by pressure oscillations. Though the mean pressure in the Cu species is greater than in the Mo species, the mean density in the Cu species is lower than in the Mo species. The reason is the thrice higher coefficient of thermal expansion of copper, as compared to that of molybdenum, for an identical temperature in both species (see Fig. 4b). Another interesting effect observed in calculations (see Fig. 4b and 4c) is the fact that the temperatures in the species become rapidly equalized after compaction of the Cu–Mo nanopowder, whereas the pressures remain different. This happens because the characteristic time of heat transfer between the copper and molybdenum nanoparticles $\tau_T \sim R_p^2$ is much smaller than the characteristic time of pressure equalization $\tau_c \sim R_s$. In addition, the pressures in the species are different owing to the action of the surface tension force proportional to the product of the surface tension coefficient and the curvature of the boundary between the species.

The structural features of dynamic deformation of the Cu–Mo nanopowder considered agree with experimental data obtained during explosive compaction of a mixture of copper and molybdenum micropowders [7]. An analysis of the Cu–Mo compact structure showed that Cu microparticles experience high strains and lose their shape [7]. Mo microparticles are weakly deformed, and extrusion of soft copper between Mo microparticles is observed. Note, the size of microparticles used in the experiment [7] was greater than the particle size in the present work by three orders of magnitude, whereas the loading pressure was two or three times smaller; for this reason, copper microparticles did not melt in [7].

As the loading intensity increases, voids appear and grow in the extended nanocell. To study this phenomenon, we performed two calculations with more intense loads ($P_v^0 = 2.6$ GPa and $P_v^1 = 0.6$ GPa; $P_v^0 = 3.6$ GPa and $P_v^1 = 1.2$ GPa) and $\tau_0 = \tau_1 = \tau_2 = 2 \cdot 10^3$ fsec and $\tau_1 = 1.5\tau_0$ (see Fig. 1). The patterns observed are identical. Interacting with the nanocell, the piston is drastically decelerated and becomes bounced from the nanocell surface (see Fig. 4a). As a result, high compressive stresses and then tensile stresses arise in the nanocell, which are responsible for origination and growth of voids. Figures 5 and 6 show the results calculated for the nanocell

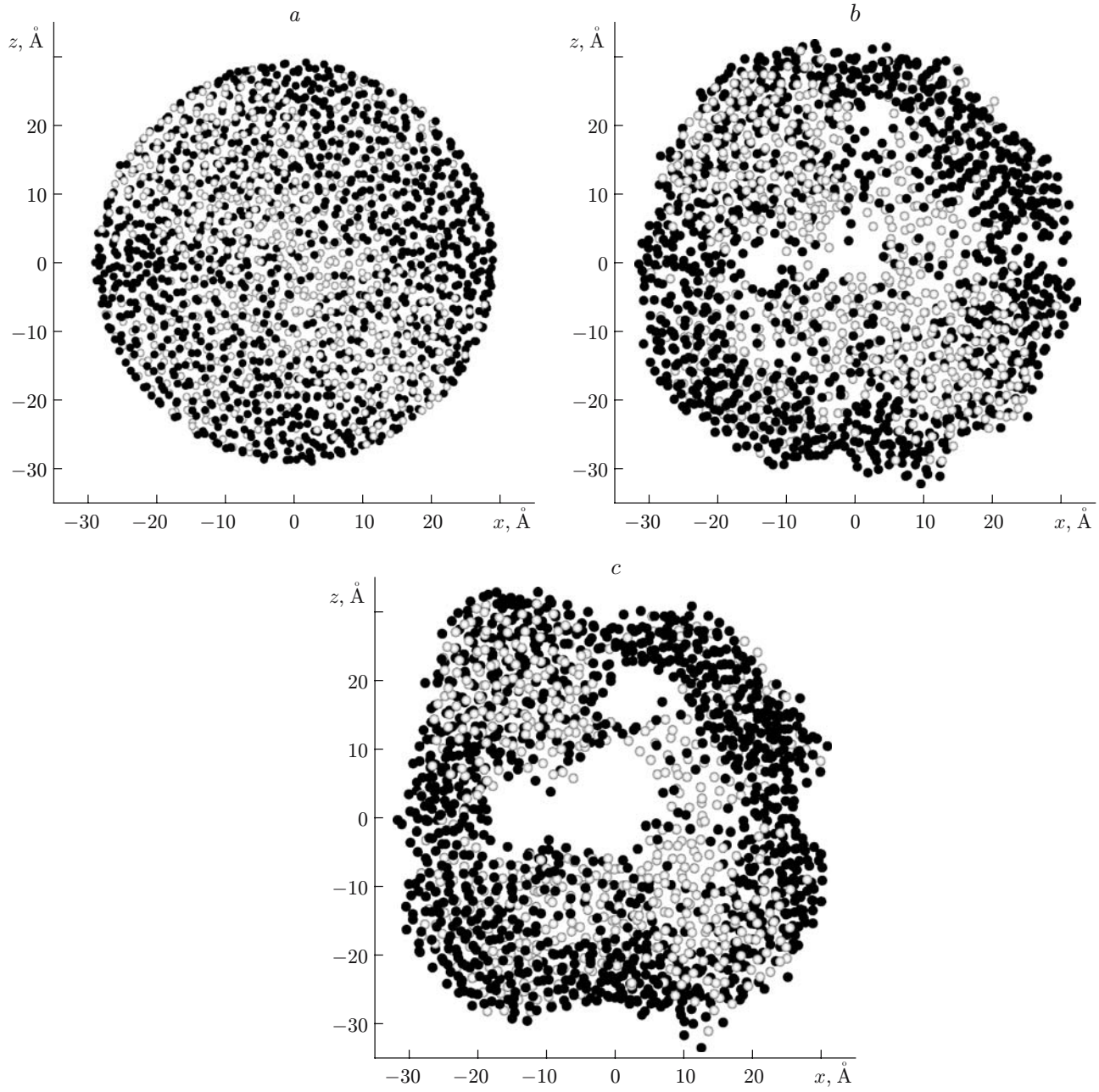

Fig. 5. Projection of nanocell atoms located in the layer -5 Å $< y < 5$ Å onto the plane (x, z) ($P_v^0 = 3.6$ GPa and $P_v^1 = 1.2$ GPa) for $t = 4.8 \cdot 10^3$ (a), $6 \cdot 10^3$ (b), and $7 \cdot 10^3$ fsec (c); notation the same as in Fig. 3.

loaded by a pressure pulse ($P_v^0 = 3.6$ GPa and $P_v^1 = 1.2$ GPa). Figure 5 shows the atomic configurations in a layer of thickness $\Delta y \approx 10$ Å at the times of compressive stresses (Fig. 5a) and tensile stresses (Figs. 5b and 5c). It is seen that the voids nucleate and grow in the copper species, whereas Mo nanoparticles remain compact (see Fig. 5b). In the course of expansion, the piston moves away from the nanocell atoms (see Figs. 4a and 5c). As Mo atoms are stronger bonded to the piston than Cu atoms, they separate from the piston later. This leads to perturbation of the nanocell surface, and it starts to deviate from the spherical shape. After piston separation, the nanocell continues to expand by inertia for a certain time. The voids coagulate, and one large void is formed in the nanocell center. This void grows proportional to the increase in nanocell volume. Moreover, perturbations of

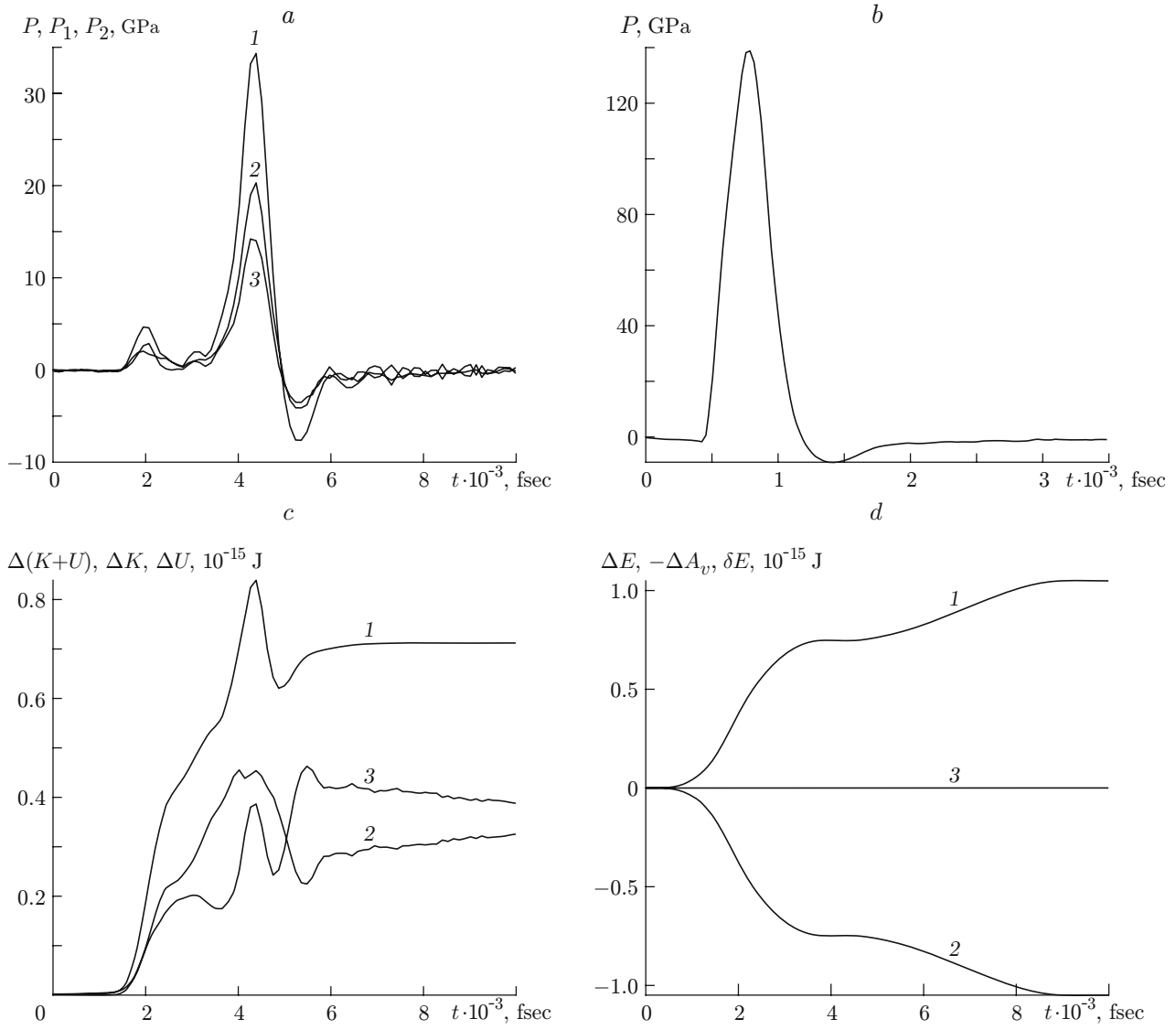

Fig. 6. Calculated mean parameters in a Cu–Mo nanocell loaded by a pressure pulse $P_v^0 = 3.6$ GPa and $P_v^1 = 1.2$ GPa: (a) $P(t)$ (1), $P_1(t)$ (2), and $P_2(t)$ (3); (b) $P(t)$ for a Cu single-crystal nanoparticle loaded by a pressure pulse; (c) $\Delta(K(t) + U(t))$ (1), $\Delta K(t) = K(t) - K(0)$ (2), and $\Delta U = U(t) - U(0)$ (3); (d) $\Delta E(t)$ (1), $-\Delta A_v(t)$ (2), and $\delta E(t)$ (3).

the nanocell surface becomes more intense with time (see Fig. 5c). To estimate the influence of piston separation on the nucleation and growth of voids, we performed calculations with twice increased numerical values of $D_{\alpha,\beta}$ [constants in the formulas for the interaction potential between the piston and the nanocell atoms (3)]. In this case, the voids again nucleated and grew in Cu nanoparticles. During the calculation, the piston did not separate from the nanocell surface, and the surface remained spherical. Note that replacement of the constants $D_{\alpha,\beta}$ in Eqs. (3) exerted only a weak effect on the dependences of the mean parameters in the nanocell on time. It is seen from Fig. 6a, which shows the time evolution of pressure in the nanocell, that the void growth occurs at a critical tensile pressure $P^* \approx -7.63$ GPa. A similar calculation of compaction of a nanocell consisting of Cu nanoparticles shows that void nucleation and growth occur at $P^*_{\mathrm{Cu}} \approx -6.39$ GPa; the corresponding value for a nanocell consisting of Mo nanoparticles is $P^*_{\mathrm{Mo}} \approx -10$ GPa. Void nucleation and growth in a Cu–Mo two-species mixture occur in the softer copper material. The critical value of the total tensile pressure in the Cu–Mo mixture, however, is higher than that in copper and lower than that in molybdenum: $|P^*_{\mathrm{Cu}}| < |P^*| < |P^*_{\mathrm{Mo}}|$. In a similar calculation with loading by a

smaller pressure pulse ($P_v^0 = 2.6$ GPa and $P_v^1 = 0.6$ GPa), we obtain $P_{\text{Cu}}^* \approx -6.86$ GPa, $P^* \approx -7.5$ GPa, and $P_{\text{Mo}}^* \approx -10.6$ GPa; a small increase in P_{Cu}^* in this case may be caused by less intense heating of the Cu species during copper nanocell compression and compaction. The same feature is observed here: the absolute critical value of the total tensile pressure in the Cu–Mo mixture is higher than that in copper and lower than that in molybdenum.

The difference between P^* and P_{Cu}^* is caused by the hardening effect of the Mo species. In the mixture, copper atoms interact not only with each other, but also with molybdenum atoms. As the potential well for the effective pair potential of interaction of Cu and Mo atoms is lower than the corresponding value for the Cu–Cu potential (see Fig. 2), the strength of the Cu–Mo mixture increases.

A problem of high-velocity ($\dot{\varepsilon} = 10^9$ sec^{-1}) three-dimensional extension of a cubic single crystal of copper preheated to $T_0 = 300$ K was solved in [13] by the molecular dynamics method. Two cases were considered: an ideal single crystal and a single crystal containing a void with a radius of 1.9 nm in the center. For the ideal single crystal of copper, the critical value of pressure at which nucleation and growth of voids begins is $|P_{\text{Cu}}^{id}| \approx 10$ GPa, whereas the critical pressure for the void-containing single crystal is $|P_{\text{Cu}}^{v}| \approx 6$ GPa. It is seen that the value of $|P_{\text{Cu}}^{v}|$ is close to the critical values of pressure calculated in the present work: $|P_{\text{Cu}}^*| \approx 6.39$–$6.86$ GPa. This is caused by substantial strains in the Cu species induced during compaction of the Cu–Mo nanocell. The voids are filled due to nanocell compression, and the crystalline structure of the Cu species is violated and becomes amorphous. Therefore, nucleation of pores in the Cu species under extension requires lower elastic energy than in the ideal single crystal of copper.

To verify this assumption, we solved a problem of pulsed loading of a spherical single crystal of copper preheated to $T_0 = 300$ K. The physical formulation of the problem is identical to that illustrated in Fig. 1, but loading of one nanoparticle of the Cu single crystal of radius $R_p = 2.7$ nm by a piston of radius $r_v^0 = 3$ nm is considered instead of eight Cu and Mo nanoparticles. The piston experiences a pressure pulse with the parameters $P_v^0 = 40$ GPa, $P_v^1 = 0.2$ GPa, $\tau_0 = 0.5 \cdot 10^3$ fsec, $\tau_1 = 10^3$ fsec, $\tau_2 = 2 \cdot 10^3$ fsec, and $\tau_3 = 0.2 \cdot 10^3$ fsec. In this case, the mean strain rate is $\dot{\varepsilon} \approx 2 \cdot 10^{11}$ sec^{-1}. The calculated dependence of pressure in the Cu nanoparticle on time is plotted in Fig. 6b. The dependence of the piston radius on time is similar to the dependence plotted by curve 4 in Fig. 4a. The piston is first accelerated; then it becomes decelerated and bounced away from the nanoparticle surface owing to interaction with Cu atoms. As a result, a shock wave is generated in the Cu nanoparticle; this wave propagates toward the center, become reflected, and reaches the nanoparticle surface. A region of tensile stresses is formed in the nanoparticle, where the voids starts to form and grow, coagulating with time into one void. It is seen from Fig. 6b that the critical value of pressure at which the voids appear in the nanoparticle of the copper single crystal is $|P_{\text{Cu}}^0| \approx 9.07$ GPa. A small difference of this value from $|P_{\text{Cu}}^{id}| \approx 10$ GPa obtained in [13] is apparently caused by substantial heating ($T \approx 2000$ K) of the Cu nanoparticle due to shock-wave loading.

Let us consider the mechanism of energy redistribution in the nanocell in the course of its compaction by the piston. Figure 6c shows the changes in the kinetic ΔK, internal ΔU, and total $\Delta(K + U)$ energy of Cu–Mo atoms with time. By comparing Figs. 6a and 6c, we can see that all three curves in Fig. 6c have peaks at the point of the maximum pressure, and the width of the peak on the dependence $\Delta U(t)$ is one third of the peak width on the curve $\Delta K(t)$. The reason is intense filling of the voids before the pressure peak at $t \approx 4.5 \cdot 10^3$ fsec, which converts the internal energy of atoms to the kinetic energy (see Fig. 6c). When the pressure peak is reached, the nanocell expands and performs the work on the piston; as a result, the piston velocity increases (see Fig. 4a), and the energy of atoms in the nanocell decreases. At the moment the voids appear, elastic unloading occurs, which leads to an increase in the internal energy ΔU. The kinetic energy continues to decrease until the voids coagulate; at this moment, the kinetic energy slightly increases owing to conversion of the internal energy to the kinetic energy. Figure 6d shows the time evolution of the inverse work of the internal pressure $-\Delta A_v$, the changes in the total energy of the system ΔE, and the numerical residue $\delta E = \Delta E - \Delta A_v$. It is seen that the growth rate of the total energy has two maximums. The first one is caused by nanocell compression due to void filling ($\Delta E = -P\Delta V > 0$, $P > 0$, and $\Delta V < 0$), and the second one is caused by nanocell expansion due to void growth ($\Delta E = -P\Delta V > 0$, $P < 0$, and $\Delta V > 0$). As was noted above, the energy conservation law is satisfied in calculations within 0.5%.

To determine the influence of the initial temperature on the compaction process, we calculated the compaction of a "cold" Cu–Mo nanocell. Before the compaction, the temperature of atoms in the "cold" nanocell was $T_0 = 0.1$ K. There were no essential differences in the calculated qualitative and quantitative features of the compaction process in the "cold" and "normal" nanocells. In the case of compaction of a "cold" nanocell, the

atomic temperature rapidly increased to $T \approx T_0 = 300$ K owing to a decrease in surface energy [4, 5], after which the compaction process proceeded in the same manner as in the "normal" nanocell.

The calculations showed that the nanocell size affects the compaction process. The loading conditions being identical, a twofold decrease in the nanocell size leads to a twofold increase in pressure and temperature of the nanocell after compaction. The observed scaling is caused by the fact that the work performed by the piston is proportional to the nanocell area: $\Delta A_v \approx P_v S\,\delta r_v$, and the temperature and pressure are inversely proportional to the nanocell volume: $T \sim P \approx \Delta E/V$. Taking into account that $\Delta E = \Delta A_v$, $S \approx l^2$, and $V \approx l^3$, we can demonstrate that the pressure after compaction is inversely proportional to the nanocell size: $P \approx P_v \delta r_v / l$.

Conclusions. Compaction of a mixture of Cu–Mo nanopowders loaded by a pressure pulse was studied by the molecular dynamics method. It was demonstrated that compaction occurs at the expense of the copper species filling the voids. Copper nanoparticles experience significant deformation and lose their shape, whereas Mo nanoparticles are only slightly deformed. A similar dependence was observed in experiments on explosive compaction of a mixture of Cu–Mo micropowders [7]. At the stage of void filling, the deformation in Cu nanoparticles has an intermittent oscillatory character.

Under intense loading during extension of the Cu–Mo compact, the voids appear and grow in the Cu species. The critical stress at which the voids are generated in the Co–Mo compact is slightly higher than in the Cu compact and lower than in the Cu single crystal. The higher strength of the Cu–Mo compact, as compared with the strength of the Cu compact, is caused by hardening of the Cu species owing to interaction of copper atoms with molybdenum atoms. The lower strength of the Cu–Mo compact, as compared with the strength of the Cu single crystal, is caused by violation of the crystalline structure and formation of the amorphous structure of the Cu species during void filling in the Cu–Mo nanocell.

This work was supported by the Russian Foundation for Basic Research (Grant No. 08-01-00108), Integration Project of the Siberian Division of the Russian Academy of Sciences (Project No. 106), Targeted Project of the Presidium of the Siberian Division of the Russian Academy of Sciences (Project No. 5), and Council on Grants of the President of the Russian Federation for Support of Young Russian Scientists and Leading Scientific Schools (Grant No. NSh-4292.2008.1).

REFERENCES

1. A. B. Sawaoka (ed.), *Shock Waves in Materials Science*, Springer-Verlag, Hong Kong–Barcelona–Budapest (1993).
2. R. Prummer, *Explosivverdichtung Pulvriger Substanzen*, Springer-Verlag, BRD (1987).
3. V. V. Ivanov, Yu. A. Kotov, A. N. Vikhrev, and N. I. Noskova, "Hot dynamic compaction of nanosize powders of aluminum and titanium oxides," *Dokl. Ross. Akad. Nauk*, **352**, No. 6, 759–761 (1997).
4. S. P. Kiselev and V. P. Kiselev, "Compaction of copper nanopowder in a shock wave," *Fiz. Mezomekh.*, **9**, No. 6, 59–70 (2006).
5. S. P. Kiselev, "Compaction of copper nanopowder," *J. Appl. Mech. Tech. Phys.*, **48**, No. 3, 412–419 (2007).
6. G. A. Shvetsov, V. I. Maly, A. G. Anisimov, et al., "High-current ARC erosion of explosively compacted Mo/Cu and W/Cu electrodes," *IEEE Trans. Magn.*, **33**, No. 1, 410–412 (1997).
7. V. I. Mali and T. S. Teslenko, "Structure and properties of explosively compacted copper–molybdenum," *Combust., Expl., Shock Waves*, **38**, No. 4, 473–477 (2002).
8. M. P. Allen and D. J. Tildesley, *Computer Simulation of Liquids*, University Press, Oxford (1987).
9. F. Cleri and V. Rosato, "Tight-binding potentials for transitions metals and alloys," *Phys. Rev. B*, **48**, 22 (1993).
10. M. A. Karolewski, "Tight-binding potentials for sputtering simulations with FCC and BCC metals," *Radiat. Effects Defects Solids*, **153**, 229–235 (2001).
11. M. Yan, V. Vitek, and S. P. Chen, "Many-body central force potentials and properties of grain boundaries in NiAl," *Acta Mater.*, **44**, 4351–4365 (1996).
12. A. V. Bolesta, "Modeling of processes at internal boundaries in metallic nanostructures," Candidate's Dissertation in Phys.-Math. Sci., Novosibirsk (2002).
13. J. Belak, "On the nucleation and growth of voids at high strain-rates," *J. Comput. Aided Mater. Design*, **5**, 193–206 (1998).